Fast Inverse Nonlinear Fourier Transforms for Fiber Bragg Grating Design and Related Problems

Sander Wahls, *Member, IEEE* and Vishal Vaibhav

arXiv:1607.01305v1 [cs.IT] 5 Jul 2016

***Abstract*—The problem of constructing a fiber Bragg grating profile numerically such that the reflection coefficient of the grating matches a given specification is considered. The well-known analytic solution to this problem is given by a suitable inverse nonlinear Fourier transform (also known as inverse scattering transform) of the specificed reflection coefficient. Many different algorithms have been proposed to compute this inverse nonlinear Fourier transform numerically. The most efficient ones require $\mathcal{O}(D^2)$ floating point operations (flops) to generate D samples of the grating profile. In this paper, two new fast inverse nonlinear Fourier transform algorithms that require only $\mathcal{O}(D\log^2 D)$ flops are proposed. The merits of our algorithms are demonstrated in numerical examples, in which they are compared to a conventional layer peeling method, the Toeplitz inner bordering method and integral layer peeling. One of our two algorithms also extends to the design problem for fiber-assisted codirectional couplers, which in turn also arises in modulation step of the nonlinear inverse synthesis method for fiber-optic communications.**

***Index Terms*—Nonlinear Fourier transform, fiber nonlinear optics, Bragg gratings, optical fiber communication**

I. Introduction

Fiber Bragg gratings are optical filters which are used in different application areas ranging from optical communications to astronomical sensing. The *coupled mode equations*

$$\frac{d}{dx}\begin{bmatrix} a(x,\lambda) \\ b(x,\lambda) \end{bmatrix} = \begin{bmatrix} i\lambda & q(x) \\ -\kappa\bar{q}(x) & -i\lambda \end{bmatrix}\begin{bmatrix} a(x,\lambda) \\ b(x,\lambda) \end{bmatrix}, \quad \begin{bmatrix} a(-L,\lambda) \\ b(-L,\lambda) \end{bmatrix} = \begin{bmatrix} 1 \\ 0 \end{bmatrix}, \tag{1}$$

describe the interaction between the forward propagating mode $a(x,\lambda)$ and the backward propagating mode $b(x,\lambda)$ in a fiber Bragg grating with the coupling profile $q(x)$ [1, Eq. 15–16]. In these equations, $x \in [-L, L]$ denotes position, $\lambda \in \mathbb{R}$ is the normalized detuning parameter, $\bar{\cdot}$ denotes the complex conjugate, and $\kappa = -1$. (Other interpretations as well as the case $\kappa = +1$ are discussed at the end of this section.) The *reflection coefficient* of the grating is given by

$$\hat{q}(\lambda) = e^{-2i\lambda L}\frac{b(L,\lambda)}{a(L,\lambda)}, \qquad \lambda \in \mathbb{R}. \tag{2}$$

The fiber Bragg grating design problem is to determine the profile $q(x)$ that leads to a given reflection coefficient $\hat{q}(\lambda)$. One popular approach to this problem is to solve the Gelfand-Levitan-Marchenko (GLM) equations [2], [3]. Many numerical algorithms for fiber Bragg grating design discretize the GLM equations in order to recover samples of the grating profile. Recently developed algorithms are able to recover D such samples using $\mathcal{O}(D^2)$ floating point algorithms *(flops)* with an approximation error that has been observed to decrease quadratically [4].

Layer peeling algorithms take a different approach. The coupled mode equations are discretized directly. Under the assumptions that the profile is piecewise constant,

$$q(x) = \sum_{n=0}^{D-1} q_n w\left(\frac{x+L}{\varepsilon} - n\right), w(x) := \begin{cases} 1, & x \in [0,1) \\ 0, & \text{otherwise} \end{cases}, \tag{3}$$

and the segment length $\varepsilon := \frac{2L}{D}$ is small, the following discretization of the coupled mode equations can be obtained:

$$\begin{bmatrix} A_{n+1}(z) \\ B_{n+1}(z) \end{bmatrix} = \frac{1}{\theta_n}\begin{bmatrix} 1 & z^{-1}\varepsilon q_n \\ -\kappa\varepsilon\bar{q}_n & z^{-1} \end{bmatrix}\begin{bmatrix} A_n(z) \\ B_n(z) \end{bmatrix}, \quad \begin{bmatrix} A_0(z) \\ B_0(z) \end{bmatrix} = \begin{bmatrix} 1 \\ 0 \end{bmatrix}, \tag{4}$$

where $z := e^{-2i\lambda\varepsilon}$ and $\theta_n := \sqrt{1+\kappa|\varepsilon q_n|^2}$. With $A(z) := A_D(z)$ and $B(z) := B_D(z)$ denoting the discrete-time *wave functions*, the resulting discrete-time approximation of the reflection coefficient $\hat{q}(\lambda)$ can be written as [5]

$$\hat{Q}(z) := z^{D/2}\frac{B(z)}{A(z)}, \qquad |z| = 1. \tag{5}$$

In the context of fiber Bragg grating, this approach is due to Feced et al. [6]. (In another context, a very similar discretization is due to Ablowitz and Ladik [7].) Layer peeling algorithms start by reconstructing q_{D-1} from a specified discrete reflection coefficient $\hat{Q}(z)$. Then, the discretized coupled mode equations are used to find the reflection coefficent that corresponds the same grating, but with $q_{D-1} = 0$, effectively reducing the length of the grating, and repeat the process until all q_n have been reconstructed. Layer peeling algorithms can be implemented using $O(D^2)$ flops as well, with an error that also vanishes quadratically.

Recall that a grating design algorithm reconstructs samples q_n of the profile $q(x)$ from a given reflection coefficient $\hat{q}(\lambda)$. The number of samples D that has to be generated can be high in some applications such as astronomical sensing [8] or, see Remark 2 below, fiber-optic communicatons [9, p. 4345]. The $\mathcal{O}(D^2)$ complexity of the known algorithms results in significant computational costs in such cases. In this

Both authors are with the Delft University of Technology, Delft Center for Systems and Control, Delft, The Netherlands, e-mail: s.wahls@tudelft.nl, v.k.vaibhav@tudelft.nl.

©2016 IEEE. Personal use of this material is permitted. Permission from IEEE must be obtained for all other uses, in any current or future media, including reprinting/republishing this material for advertising or promotional purposes, creating new collective works, for resale or redistribution to servers or lists, or reuse of any copyrighted component of this work in other works.

paper, therefore two new, fundamentally faster layer peeling algorithms are proposed. They require only $\mathcal{O}(D \log^2 D)$ flops, which is close to a conventional FFT.

Remark 1. By choosing $\kappa = +1$ instead of -1 in the coupled mode equations, the design problem for fiber-assisted codirectional couplers is obtained [10].

Remark 2. The reflection coefficient furthemore also constitutes a *nonlinear Fourier transform* that can be used to solve the nonlinear Schrödinger equation with initial condition $q(x)$ in closed-form [11]. This fact is currently receiving much attention in the area of fiber-optic communications, where the Schrödinger equation models an ideal lossless fiber [9], [12]. The fiber Bragg grating design becomes an *inverse nonlinear Fourier transform* in this context. The results in this paper can in particular accelerate the modulation step in the *nonlinear inverse synthesis* method [12], and therefore complement the paper [13] in which already the demodulation step has been accelerated using fast nonlinear Fourier transforms [14], [15]. For the sake of readibility, we will however limit our discussion to the fiber Bragg grating design problem as far as possible, for which most of our benchmark algorithms have been developed.

The rest of the paper is structured as follows. In the next section, the new algorithms are derived. Then, in Section III, the new algorithms are compared to several current state-of-the-art algorithms in numerical examples. The paper is finally concluded in Section IV.

II. Fast Inverse Nonlinear Fourier Transform

The numerical computation of the reflection coefficient consists of two stages: First, compute the wave functions $A(z)$ and $B(z)$ from the samples $q_0, q_1, \ldots, q_{D-1}$; and second, evaluate (5) at D frequencies of interest. Our algorithms are based on reversing this process [16]. They use the provided reflection coefficient to synthesize suitable wave functions via interpolation, and then recover the samples using layer peeling. The synthesis of the wave functions hereby is the tricky part. The main difficulty is that the wave functions cannot be chosen arbitrarily. In practice, gratings are always of finite length $D\varepsilon$. This amounts to finitely many samples in the coupled mode equations. It follows from (4) that

$$A(z) = \sum_{i=0}^{D-1} A_i z^{-i} \text{ and } B(z) = \sum_{i=0}^{D-1} B_i z^{-i} \tag{6}$$

have to be polynomials of degree $D-1$. Since layer peeling is based on inverting (4), there should exist samples $q_0, q_1, \ldots, q_{D-1}$ that, when plugged into (4), actually lead to the generated wave functions. Otherwise, the task of recovering such samples is ill-posed, and the layer peeling step may suffer from numerical instabilities. Skaar and his coworkers have coined the term *realizability* for this issue [17], [10]. They showed that the wave functions in (6) can be generated through (4) for a suitable choice of samples $q_0, q_1, \ldots, q_{D-1}$ if and only if the three conditions

$$|A(z)|^2 + \kappa |B(z)|^2 = 1 \text{ whenever } |z| = 1, \tag{7}$$

$$A(z) \neq 0 \text{ whenever } |z| > 1, \tag{8}$$

$$A_0 \text{ is real and non-negative} \tag{9}$$

are satisfied. (The same results have also been found in [18], [19].) We remark that many layer peeling algorithms work directly with the reflection coefficient instead of the wave functions. The issue of realizability however remains also in this case because not all reflection coefficients correspond to a finite-length grating with the desired length.

Algorithm 1 Prototype for the fast inverse NFTs

Input: Reflection coefficient $\hat{q}(\lambda)$, grating length $2L$, number of samples D

Output: Samples q_n s.t. $\hat{Q}(z)$ given in (5) satisfies (10)

1) *Synthesis:* Construct $A(z)$ and $B(z)$ such that, under consideration of (5) and the coordinate transform $z = e^{-2i\lambda\varepsilon}$, $\hat{Q}(z)$ is a "good" approximation of $\hat{q}(\lambda)$.
2) *Layer peeling:* Recover the samples q_n from $A(z)$ and $B(z)$ using fast layer peeling as in [25], [5].

Existing layer peeling methods are not adequately taking realizability into account. They either completely ignore the fact that the generated grating has to be of finite length [6], [20], [21], [22], or they do not ensure that the resulting discrete-time relizability conditions (7)–(9) are satisfied [17], [23]. Instead, the corresponding continuous-time realizability conditions are used to determine the continuous-time wave functions $b(L, \lambda)$ and $a(L, \lambda)$, and the discrete-time wave funcations $A(z)$ and $B(z)$ are found by approximating them subject to the coordinate transform $z = e^{-2i\lambda\varepsilon}$. The synthesized discrete-time wave functions usually still satisfy (7)–(9) approximately, but not exactly. The mismatch to realizability can be interpreted as measurement noise. Since layer peeling is known to be sensitive again measurement noise especially for strong gratings [24], the applicability of conventional layer peeling methods is limited by this issue.

Algorithm 1 shows the prototype for our fast inverse nonlinear Fourier transforms. Both algorithms use the same fast layer peeling step due to McClary [25], which requires only $\mathcal{O}(D \log^2 D)$ flops and has already been used successfully for another type of fast inverse nonlinear Fourier transform in [5]. The *synthesis step* will however be different, as is explained below. Note that McClary himself mentioned that his algorithm is unstable in the presence of mesurement noise. However, in our context measurement noise is equivalent to violating the realizability conditions. Therefore, we will focus especially on fulfilling them during synthesis.

A. Outline of Synthesis via Interpolation

In this paper, the synthesis step of finding suitable wave functions that will serve as inputs for the layer peeling step

is based on solving the interpolation conditions (see [16])

$$\hat{Q}(z_n) = \hat{q}(\lambda_n), \qquad n = 0, 1, \ldots, D-1, \tag{10}$$

where $\lambda_n = -\frac{\pi}{2\varepsilon} + (n+0.5)\delta$, $\delta = \frac{2\pi}{\varepsilon D} = \frac{\pi}{L}$, and $z_n = e^{-2i\lambda_n \varepsilon}$. That is, we generate wave functions such that the corresponding discrete-time reflection coefficient matches the continuous-time specification on a frequency grid. Our goal is thus to generate wave functions that solve the interpolation problem (10) and, in light of the discussion above, satisfy the three realizability conditions (7)–(9).

Remark 3. Due to discretization errors and mismatches at frequencies that are not on the grid, fulfilling the interpolation conditions does not guarantee an exact match with the desired continuous-time reflection coefficient.

An important but well-known insight used in the following is that the realizability conditions (7)–(9) are the definition of $A(z)$ being a canonical spectral factor (see [26]) of

$$|A(z)|^2 = 1 - \kappa |B(z)|^2 = \frac{1}{1 + \kappa |\hat{Q}(z)|^2}. \tag{11}$$

Therefore, $A(z)$ can be recovered using spectral factorization. The Hilbert transform (or Kolmogorov) method is especially popular to this end since it can be computed efficiently using the fast Fourier transform (FFT) [27, B4].

B. First Algorithm: Iterative Synthesis

While solving the interpolation problem (10) subject to the realizability conditions (7)–(9) is difficult in general, solving the closely related interpolation problem

$$z_n^{D/2} \frac{B(z_n)}{|A(z_n)|} = \hat{q}(\lambda_n) \tag{12}$$

subject to realizability has been shown to be simple in [16], where a closed-form formula for a suitable $B(z)$ has been given. The corresponding $A(z)$ is then found via spectral factorization. The resulting reflection coefficient (5) will have the desired magnitudes, but its phases will be incorrect. Our idea is to iteratively solve simple interpolation problems of the form (12) while adapting the phases such that the phase mismatch is reduced more and more. We start by initializing auxiliary interpolation targets $\sigma_n := z_n^{-D/2} \hat{q}(\lambda_n)$, and iterate the following steps several times.

1) Find $B(z)$ [as in (6)] by solving the interpolation problem $B(z_n) = \sigma_n / \sqrt{1 + \kappa |\sigma_n|^2}$ (see [16, IV.B]).
2) Construct the Laurent polynomial

$$\Phi(z) = \sum_{i=-D+1}^{D-1} \Phi_i z^{-i} = 1 - \kappa B(z) \bar{B}(\bar{z}^{-1}). \tag{13}$$

3) Perform a polynomial spectral factorization of $\Phi(z)$. The result constitutes $A(z)$ [as in (6)].
4) Update $\sigma_n \leftarrow \hat{q}(\lambda_n) \exp[i \angle A(z_n)]$.

Note that all steps can be implemented efficiently using the *fast Fourier transform (FFT)* [28, 8]. For the Steps 1 and 2, exploit the relation between discrete-time Fourier series and transform [28, 7.3]. Step 3 can be solved efficiently using $\mathcal{O}(OD \log(OD))$ flops, where O is an oversampling factor, using the Kolmogorov (or Hilbert transform) method for spectral factorization [27, B4]. We performed only three iterations in the numerical examples, in which case the total cost of this method remains $\mathcal{O}(OD \log(OD))$ flops.

C. Second Algorithm: Direct Synthesis

In our second algorithm, the synthesis step first generates $A(z)$ and then $B(z)$ through the following steps.

1) Find the polynomial $\phi(z) = \sum_{i=0}^{D-1} \phi_i z^{-i}$ that satisfies $\phi(z_n) = 1/\sqrt{1 + \kappa |q(\lambda_n)|^2}$ [see (11)].
2) Construct the Laurent polynomial

$$\Phi(z) = \sum_{i=-D+1}^{D-1} \Phi_i z^{-i} = \phi(z) \bar{\phi}(\bar{z}^{-1}). \tag{14}$$

3) Perform a polynomial spectral factorization of $\Phi(z)$. The result constitutes $A(z)$ [as in (6)].
4) Construct $B(z)$ [as in (6)] by solving the interpolation problem $B(z_n) = z_n^{-D/2} A(z_n) \hat{q}(\lambda_n)$.

The computational complexity is again $\mathcal{O}(OD \log^2(OD))$ if the FFT is used. We do not iterate in this synthesis method.

D. Comparison of the Two Synthesis Methods

The advantage of the iterative synthesis method is that the relizability conditions are met exactly after each iteration. We shall see later that this improves the numerical reliability of the overall inverse nonlinear Fourier transform. Its disadvantage is that it only works reliably for the case $\kappa = -1$ (cf. Remark 1). For $\kappa = +1$, the Laurent polynomial (13) will in general no longer satisfy $\Phi(z) \geq 0$ for $|z| = 1$. This is a necessary condition for the spectral factorization, which then breaks down. The direct method avoids this problem since (14) satisfies $\Phi(z) \geq 0$ for $|z| = 1$ by construction. It is therefore also applicable in the case $\kappa = +1$. However, the realizability condition (7) is only guarantueed to be satisfied at the points $z = z_n$. It may not hold for other points $z \notin \{z_n\}$, leading to less numerical robustness.

III. Numerical Examples

In this section, we compare our new fast algorithms with conventional ones in several numerical examples.

A. Overview of the Algorithms

1) Fast Iterative Algorithm: This is Algorithm 1 with the synthesis step from Section II-B. The oversampling factor used was $O = 8$. Three iterations were performed in each run. Among the three iterations, the wave functions that lead to the lowest mismatch in (10) in the squared sense was used.

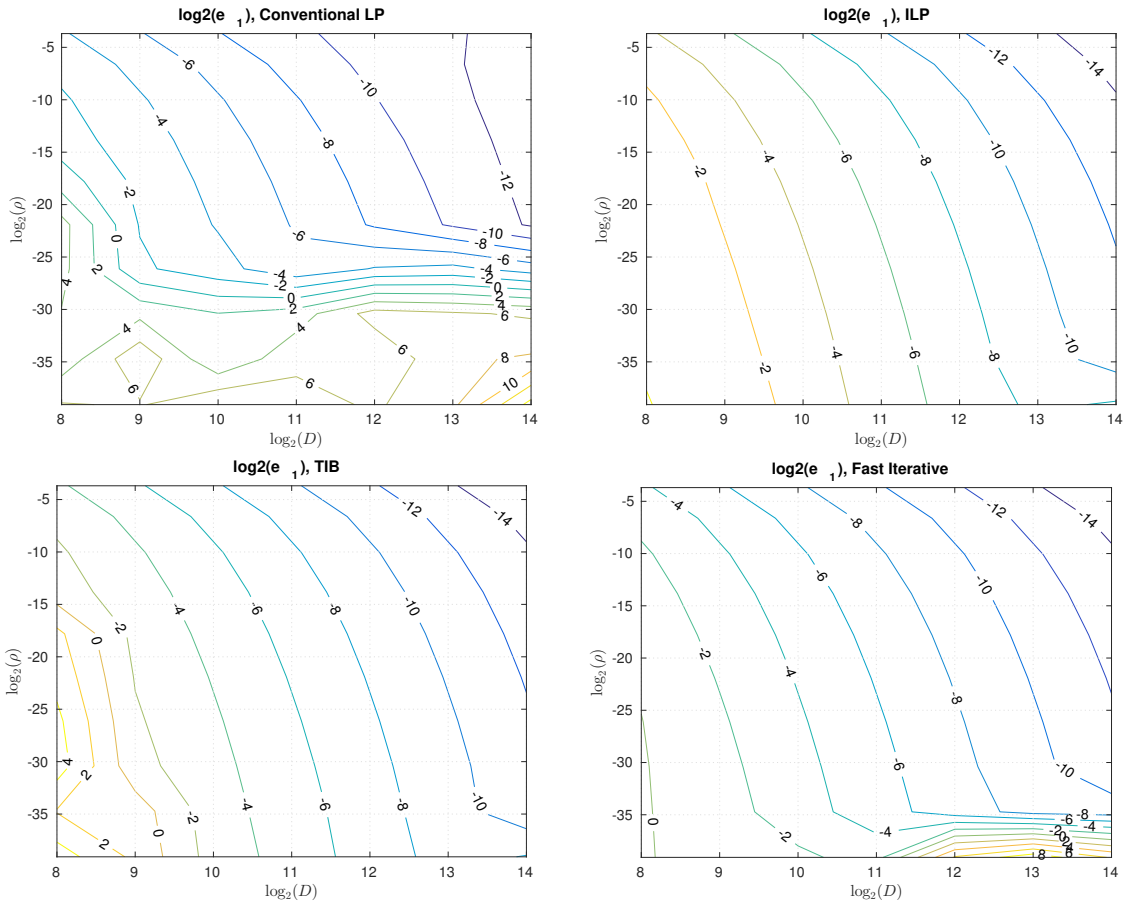

Figure 1. Simulation results for the hyperbolic secant with $L = 2$.

2) Fast Direct Algorithm: This is Algorithm 1 with the synthesis step from Section II-C and $O = 8$.

3) Conventional Layer Peeling (LP): This is the algorithm described by Skaar and Waagaard in [17, p. 1241]. They mention that a few iterations of steps 3 to 5 in their algorithm sometimes lead to improved results. In our results, iterating however could result in numerical instabilities and we performed only the one run that is necessary. The FIR approximations in the Steps 4 and 7 were implemented using a FFT. The remaining operations were implemented using oversampled FFTs with an oversampling factor of eight. In the last step, layer peeling was used to generate the samples. The complexity of this algorithm is $\mathcal{O}(D^2)$.

4) Toeplitz Bordering Method (TIB): This is the method to solve the GLM equations described in Belai et al. in [4]. The complexity of this algorithm is also $\mathcal{O}(D^2)$.

5) Integral Layer Peeling (ILP): This the algorithm by Rosenthal and Horowitz from [29]. Is was sped up using the Born approximation as described in [29, IV]. Each layer contained only one sample point for maximal accuracy, leading to an overall complexity of $\mathcal{O}(D^2 \log D)$.

B. Error critera

In order to assess the performance of the different algorithms, two different errors will be considered.

1) The first error compares the samples q'_n generated by the algorithm to known exact values $q_n = q(n\varepsilon + \frac{\varepsilon}{2})$,
$$e_1 = \left(\sum_{n=0}^{D-1} |q_n - q'_n|^2\right) / \left(\sum_{n=0}^{D-1} |q_n|^2\right). \qquad (15)$$
Note that the shift of $\varepsilon/2$ in the sample location is essential for achieving a quadratic error [30, p. 175].
2) For the second error, the samples q'_n generated by the algorithm are used to generate a piecewise constant grating $q'(x)$ as in (3). The reflection coefficient $\hat{q}'(\lambda)$ of this piecewise constant grating can be computed exactly (up to finite precision effects) using the T-matrix method [31], [32]. The difference between the reflection coefficient of this piecewise constant grating to the specified reflection coefficient is measured as
$$e_2 = \left(\sum_{n=0}^{D-1} |\hat{q}(\lambda_n) - \hat{q}'_n(\lambda_n)|^2\right) / \left(\sum_{n=0}^{D-1} |\hat{q}_n(\lambda_n)|^2\right), \qquad (16)$$
where $\lambda_n = \lambda_{-1} + (n + \frac{1}{2})\delta$ with $\delta = \frac{\lambda_D - \lambda_{-1}}{D}$. The constants λ_{-1} and λ_D will be specified per problem.

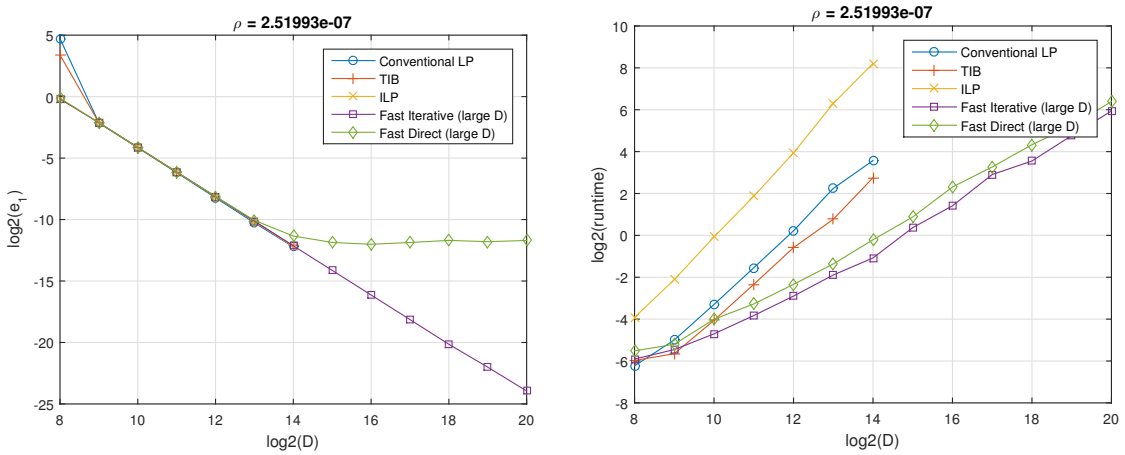

Figure 2. Errors and runtimes for the hyperbolic secant example with ρ fixed.

The error e_1 is simple to compute, but it can only be evaluated if the desired profile $q(x)$ is known analytically. Furthermore, it is not necessarily the error one is interested in practice because it is taken in the spatial domain. The error e_2 seems more relevant because it quantifies the difference between the specification and the reflection coefficent of a piecewise uniform grating realized using the output of the algorithm of interest. The disadvantage is that the terms $\hat{q}'(\lambda_n)$ in e_2 have to be computed numerically. Errors made while computing $\hat{q}'(\lambda_n)$ from the generated samples will turn up in e_2 even though they are not caused by the actual algorithm of interest. Furthermore, computing the $\hat{q}'(\lambda_n)$ requires $\mathcal{O}(D^2)$ flops, which can be significant.

C. First Example: Hyberbolic Secant, $\kappa = -1$

We first consider the example given in [4, Sec. 4]. The spatial profile we try to recover is given by

$$q(x) = \frac{\mathcal{Q}}{\mathcal{L}} \left(\operatorname{sech}(\frac{x}{\mathcal{L}})\right)^{1-2i\mathcal{F}},$$

where $\mathcal{F}$, $\mathcal{L}$ and $\mathcal{Q}$ are scalar parameters. We used $\mathcal{F} = 1.5$, $\mathcal{L} = \frac{1}{25}$, and varied $\mathcal{Q}$ from 0.5 to 5.5 in steps of 0.5. The corresponding reflection coefficient is known to be

$$\hat{q}(\lambda) = -2^{-2i\mathcal{F}}\mathcal{Q}\frac{\Gamma(d)\Gamma(f_-)\Gamma(f_+)}{\Gamma(\bar{d})\Gamma(g_-)\Gamma(g_+)},$$

where $\Gamma(\cdot)$ is the gamma function, $d = \frac{1}{2}+i(\lambda\mathcal{L}-\mathcal{F})$, $f_\pm = \frac{1}{2} - i(\lambda\mathcal{L} \pm \sqrt{\mathcal{F}^2+\mathcal{Q}^2})$, and $g_\pm = 1 - i(\mathcal{F} \pm \sqrt{\mathcal{F}^2+\mathcal{Q}^2})$. The maximum reflectivity in this example is $\rho = 1 - |\hat{q}(0)|$.

The resulting error e_1 [see (15)] is shown in Figure 1 as a function of the maximum reflectivity ρ and the number of samples D for different algorithms. Our direct synthesis algorithm is not shown in this example because it performed very similar to conventional layer peeling. All algorithms perform worse as the maximum reflectivity increases, but our algorithm breaks down much later than conventional layer peeling. Integral layer peeling and Toeplitz inner bordering however did not break down for any of the considered values of $\mathcal{Q}$, illustrating higher robustness at very high reflectivities.

A comparison of the error for a fixed ρ is shown in Figure 2 (left). Only the fast algorithms have been benchmarked for $D > 2^{14}$ samples because the conventional algorithms started to take very long. While all algorithms perform similar for $D \leq 2^{14}$, it is interesting to note that the direct method hits an error floor while the iterative method keeps improving. We attribute this to the fact that the direct algorithm does not ensure that the realizability conditions (7)–(9) are met exactly, which leads to an error in the layer peeling step. The runtimes of the algorithms are shown in Figure 2 (right). Our fast methods achieve an almost linear increase in runtime as predicted, while the conventional algorithms exhibit quadratically growing runtimes.

D. Second Example: Eight Raised Cosines, $\kappa = -1$

This example is inspired by the numerical examples in [8] and [23]. The specified reflection coeffcient is

$$\hat{q}(\lambda) = (1-\rho)\sum_{k=0}^{7} e^{i\phi_k} r(\lambda - c_k),$$

where the centers are $c_k = -3.5 + k$, the phases ϕ_k are randomly chosen from the set $\{\pm 0.25\pi, \pm 0.75\pi\}$, and

$$r(\lambda) = \begin{cases} 1, & |\lambda| \leq \frac{1-\beta}{2W} \\ \frac{1}{2} + \frac{1}{2}\cos\left(\frac{\pi W}{\beta}(|\lambda| - \frac{1-\beta}{2W})\right), & \frac{1-\beta}{2W} < |\lambda| \leq \frac{1+\beta}{2W} \\ 0, & \text{otherwise} \end{cases}$$

is a normalized raised cosine filter with width $W = 2$ and roll-off factor $\beta = 0.5$. The maximal reflectivity is $\rho = 2^{-k}$, where $k = 1, \ldots, 14$.

The resulting error e_2 [see (16)] is shown in Figure 3, again for different number of samples D and maximum reflectivities ρ. The observations are the same as in the previous example. Our fast iterative algorithm is more robust than conventional layer peeling, but less robust than integral layer peeling and Toeplitz inner bordering. We however note that the robustness of our algorithms (and conventional layer peeling) can be improved. Figure 4 (left) shows a

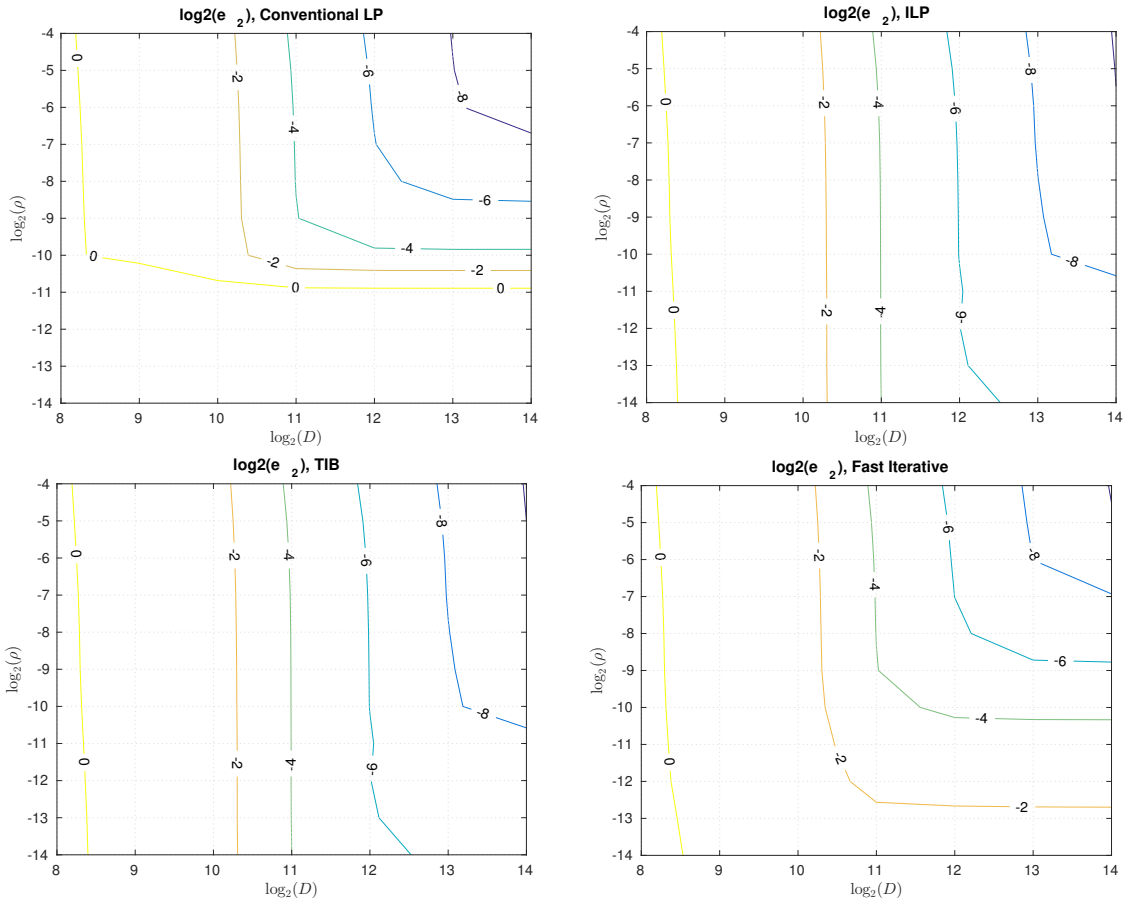

Figure 3. Simulation results for the eight raised cosines with $\kappa = -1$, $L = 200$, $\lambda_{-1} = -5$ and $\lambda = 5$.

typical case close to a breakdown, which is heralded though "aritifical tails" in the generated grating profile. (Similar observations have been made in [8, Fig. 1].) We suspect that this phenomenon is a manifestation of a truncation error in the spatial domain, i.e., the grating coefficient $q(x)$ specified through the reflection coefficient $\hat{q}(\lambda)$ is non-zero for locations outside the interval $[-L, L]$ that is considered by the inverse nonlinear Fourier transform algorithm. By doubling L, we could get rid of the artificial ripple, as is shown in Figure 4 (right). Figure 5 shows the error e_2 for both values of L. The plots confirm that double L improves the numerical accuracy of our fast iterative method such that it is very close to integral layer peeling and Toeplitz inner bordering. Note that the final error of the latter methods however slightly increases when L is doubled. We attribute this to the reduced resolution ε in the spatial domain which could be brought back to its original value by doubling the number of samples D. We remark that for our fast algorithms, this would only double the computational costs, while it would quadruple it for the conventional algorithms.

E. Third Example: Eight Raised Cosines, $\kappa = +1$

In our last example, we consider a positive sign κ in the coupled mode equations, which corresponds to a codirectional coupler (see Remark 1). The reflection coefficient was

$$\hat{q}(\lambda) = \rho \sum_{k=0}^{7} e^{i\phi_k} r(\lambda - c_k),$$

where all values are as in the previous example expect that $\rho = 2^k$ for $k = -2, -1, \ldots, 8$. [Note that while reflection coefficients cannot have absolute values larger than one if κ is negative due to (7), this is well possible if κ is positive.] The algorithms were adapted by simply changing signs were necessary. The resulting errors are shown in Figure 6. The errors of all algorithms increase with the maximum absolute value ρ of the reflection coefficient, but surprisingly this time integral layer peeling breaks down first. We do not have a good explanation for this phenomenon at the moment. Conventional layer peeling also breaks down early, while no breakdown can be observed for Toeplitz inner bordering and our fast direct method. Both methods perform equally well. Our fast iterative method breaks down before conventional layer peeling and is therefore not shown.

IV. Conclusion

In this paper, two new fast inverse nonlinear Fourier transform algorithms for fiber Bragg grating design and related

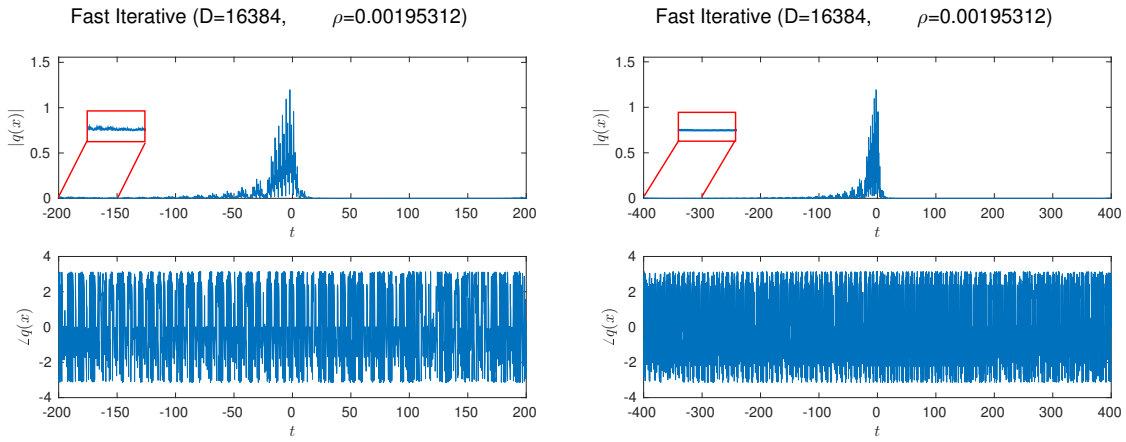

Figure 4. Grating profile generated by the fast iterative algorithm for the eight raised cosines with $\rho = 2^{-9}$ fixed, $\kappa = -1$, $\lambda_{-1} = -5$ and $\lambda_D = 5$. Left: With default value $L = 200$. Right: $L = 400$. The red boxes contain zoom-in's.

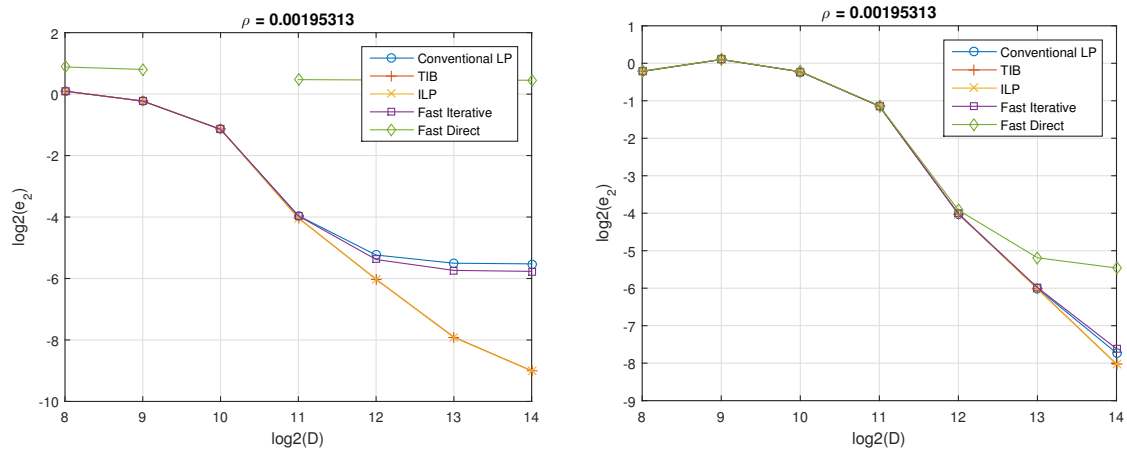

Figure 5. Errors for the raised cosines with $\rho = 2^{-9}$ fixed, $\kappa = -1$, $\lambda_{-1} = -5$ and $\lambda = 5$. Left: With default value $L = 200$. Right: $L = 400$.

problems in codirectional couplers and fiber-optic communications have been proposed and evaluated in numerical experiments. Both algorithms require only $\mathcal{O}(D \log^2 D)$ flops, D being the number of samples, which is almost an order of magnitude faster than conventional algorithms. The first prosed palgorithm is iterative and excels if the sign κ in the coupled mode equations is negative, in which case is both faster and more robust than conventional layer peeling. Although our first algorithm still broke down earlier than integral layer peeling and Toeplitz inner bordering, both of which are based on discretizing the GLM equations, it also turned out that the breakdown could be avoided by increasing the grating length. A detailed investigation of this issue and associated trade-offs is left for future research. The second proposed algorithm is direct and excels for positive κ. In our example it performed as good as the best conventional algorithm while being significantly faster.

References

[1] T. Erdogan, "Fiber grating spectra," *J. Lightwave Technol.*, vol. 15, pp. 1277–1294, Aug. 1997.

[2] V. F. Zakharov and A. B. Shabat, "Exact theory of two-dimensional self-focusing and one-dimensional self-modulation of waves in nonlinear media," *Sov. Phys. JETP*, vol. 34, pp. 62–69, Jan. 1972.

[3] G.-H. Song and S.-Y. Shin, "Design of corrugated waveguide filters by the Gel'fand-Levitan-Marchenko inverse-scattering method," *J. Opt. Soc. Am. A*, vol. 2, pp. 1905–1915, Nov. 1985.

[4] O. V. Belai, L. L. Frumin, E. V. Podivilov, and D. A. Shapiro, "Efficient numerical method of the fiber Bragg grating synthesis," *J. Opt. Soc. Am. B*, vol. 24, no. 7, pp. 1451–1457, 2007.

[5] S. Wahls and H. V. Poor, "Fast inverse nonlinear Fourier transform for generating multi-solitons in optical fiber," in *Proc. IEEE Int. Symp. Inf. Theory (ISIT)*, (Hong Kong, China), pp. 1676–1680, June 2015.

[6] R. Feced, M. N. Zervas, and M. A. Muriel, "An efficient inverse scattering algorithm for the design of nonuniform fiber Bragg gratings," *IEEE J. Quant. Electron.*, vol. 35, pp. 1105–1115, Aug. 1999.

[7] M. J. Ablowitz and J. F. Ladik, "A nonlinear difference scheme and inverse scattering," *Stud. Appl. Math.*, vol. 55, pp. 213–229, Sept. 1976.

[8] A. Buryak, J. Bland-Hawthorn, and V. Steblina, "Comparison of inverse scattering algorithms for designing ultrabroadband fibre Bragg gratings," *Optics Express*, vol. 17, no. 3, pp. 1995–2004, 2009.

[9] M. I. Yousefi and F. R. Kschischang, "Information transmission using the nonlinear Fourier transform, Parts I–III," *IEEE Trans. Inf. Theory*, vol. 60, pp. 4312–4369, July 2014.

[10] J. K. Brenne and J. Skaar, "Design of grating-assisted codirectional couplers with discrete inverse-scattering algorithms," *J. Lightwave Technol.*, vol. 21, pp. 254–263, Jan. 2003.

[11] M. J. Ablowitz, D. J. Kaup, A. C. Newell, and H. Segur, "The inverse

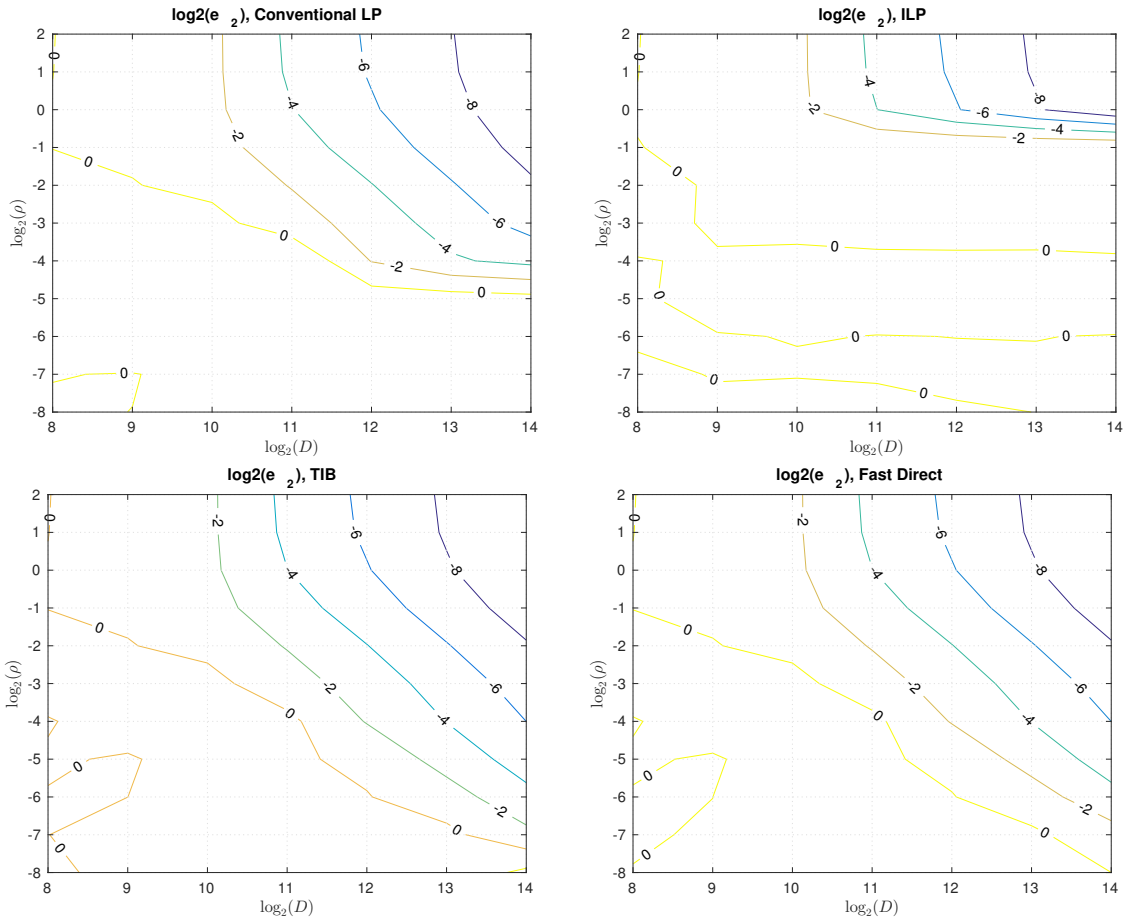

Figure 6. Simulation results for the eight raised cosines with $\kappa = +1$, $\lambda_{-1} = -5$ and $\lambda_D = 5$.

scattering transform – Fourier analysis for nonlinear problems," *Stud. Appl. Math.*, vol. 53, pp. 249–315, 1974.

[12] J. E. Prilepsky, S. A. Derevyanko, K. J. Blow, I. Gabitov, and S. K. Turitsyn, "Nonlinear inverse synthesis and eigenvalue division multiplexing in optical fiber channels," *Phys. Rev. Lett.*, vol. 113, July 2014. article no. 013901.

[13] S. T. Le, S. Wahls, D. Lavery, J. E. Prilepsky, and S. K. Turitsyn, "Reduced complexity nonlinear inverse synthesis for nonlinearity compensation in optical fiber links," in *Proc. Conf. on Lasers & Electro-Optics/Europe (CLEO/EU)*, (Munich, Germany), June 2015.

[14] S. Wahls and H. V. Poor, "Introducing the fast nonlinear Fourier transform," in *Proc. IEEE Int. Conf. Acoust. Speech Signal Process. (ICASSP)*, (Vancouver, Canada), pp. 5780–5784, May 2013.

[15] S. Wahls and H. V. Poor, "Fast numerical nonlinear Fourier transforms," *IEEE Trans. Inf. Theory*, vol. 61, pp. 6957–6974, Dec. 2015.

[16] S. Wahls and H. V. Poor, "Inverse nonlinear Fourier transforms via interpolation: The Ablowitz-Ladik case," in *Proc. Int. Symp. Math. Theory Netw. Syst. (MTNS)*, (Groningen, The Netherlands), pp. 1848–1855, July 2014.

[17] J. Skaar and O. H. Waagaard, "Design and characterization of finite-length fiber gratings," *IEEE J. Quant. Electron.*, vol. 39, pp. 1238–1245, Oct. 2003.

[18] T. Tao and C. Thiele, "Nonlinear Fourier analysis." Lect. Notes IAS Park City Summer School, July 2003. arXiv:1201.5129v1.

[19] Y.-J. Tsai, *$SU(2)$ Nonlinear Fourier Transform*. Dissertation, UCLA, Los Angeles, CA, 2005. http://search.proquest.com/docview/305033060.

[20] J. Skaar, L. Wang, and T. Erdogan, "On the synthesis of fiber Bragg gratings by layer peeling," *IEEE J. Quant. Electron.*, vol. 37, no. 2, pp. 165–173, 2001.

[21] L. Poladian, "Simple grating synthesis algorithm," *Optics Lett.*, vol. 25, no. 11, pp. 787–789, 2000.

[22] L. Dong and S. Fortier, "Formulation of time-domain algorithm for fiber Bragg grating simulation and reconstruction," *IEEE J. Quant. Electron.*, vol. 40, pp. 1087–1098, Aug. 2004.

[23] M. I. Yousefi and X. Yangzhang, "Linear and nonlinear frequency-division multiplexing." Preprint, May 2016. arXiv:1603.04389 [cs.IT].

[24] J. Skaar and R. Feced, "Reconstruction of gratings from noisy reflection data," *JOSA A*, vol. 19, no. 11, pp. 2229–2237, 2002.

[25] W. K. McClary, "Fast seismic inversion," *Geophysics*, vol. 48, pp. 1371–1372, Oct. 1983.

[26] A. H. Sayed and T. Kailath, "A survey of spectral factorization methods," *Numer. Linear Algebra Appl.*, vol. 8, pp. 467–496, 2001.

[27] B. Dumitrescu, *Positive Trigonometric Polynomials and Signal Processing Applications*. Springer, 2007.

[28] D. G. Manolakis and V. K. Ingle, *Applied Digital Signal Processing*. Cambridge Univ. Press, 2011.

[29] A. Rosenthal and M. Horowitz, "Inverse scattering algorithm for reconstructing strongly reflecting fiber Bragg gratings," *IEEE J. Quant. Electron.*, vol. 39, pp. 1018–1026, Aug. 2003.

[30] S. Burtsev, R. Camassa, and I. Timofeyev, "Numerical algorithms for the direct spectral transform with applications to nonlinear Schrödinger type systems," *J. Comput. Phys.*, vol. 147, pp. 166–186, Nov. 1998.

[31] M. Yamada and K. Sakuda, "Analysis of almost-periodic distributed feedback slab waveguides via a fundamental matrix approach," *Appl. Optics*, vol. 26, no. 16, pp. 3474–3478, 1987.

[32] G. Boffetta and A. R. Osborne, "Computation of the direct scattering transform for the nonlinear Schroedinger equation," *J. Comput. Phys.*, vol. 102, pp. 252–264, Oct. 1992.